Physics – Uspekhi **52** (9) 879 – 890 (2009)

INSTRUMENTS AND METHODS OF INVESTIGATION PACS numbers: 29.40.Vj, **95.40.+s**, 95.55.Vj

Electron–proton separation in calorimetry experiments directly measuring the composition and energy spectrum of cosmic rays

S A Voronov, S V Borisov, A V Karelin

DOI: 10.3367/UFNe.0179.200909b.0931

Contents

Abstract. Calorimetric particle detectors that play an important role in high-energy cosmic-ray balloon and satellite experiments not only have the major task of measuring energy but also face the problem of identifying electrons and protons. This problem is usually solved by measuring the longitudinal and traverse shower profiles and the total energy release in the calorimeter, using the fact that electromagnetic and hadronic showers differ in their spatial and energy distributions. In this paper, electron and proton identification methods for different types of calorimeters used in cosmic-ray balloon- and satellite-borne experiments are discussed.

1. Introduction

The influence of cosmic rays on several physical processes at work on Earth had been apparent long before they were discovered in 1912. The first device used to record such influence was a simple electrically charged metal cylinder that lost the charge (under the effect of cosmic radiation, as shown only after discovering the latter) much sooner than if the loss had been due only to imperfections in the insulator material covering the cylinder. This phenomenon was first described by Sh Coulomb (see Ref. [1]) in 1785, but physicists could not explain it until late in the 19th century (i.e., until the discovery of radioactivity).

Early experiments designed to study ionizing radiation in the atmosphere used electrometers and ionization chambers (for example, the experiments of Theodore Wulf, a German physicist, at the top of the Eiffel Tower, Paris, in 1910 [2] and the famous Hess experiment [3] in 1912).

S A Voronov, S V Borisov, A V Karelin
MEPhI National Research Nuclear University
Kashirskoe shosse 31, 115409 Moscow, Russian Federation
Tel. (7-495) 323 92 51
E-mail: sergvor@gmail.com, stanislav.r2@gmail.com, karelin@hotbox.ru

Received 29 December 2008, revised 10 March 2009
Uspekhi Fizicheskikh Nauk **179** (9) 931 – 944 (2009)
DOI: 10.3367/UFNr.0179.200909b.0931
Translated by Yu V Morozov; edited by A Radzig

Further cosmic ray investigations were carried out with other types of detectors as well. The publications by D W Skobeltzin [4] (see also Ref. [5]) in the 1920–1930s opened up a wide range of applications of the Wilson chamber placed in a magnetic field. W Bothe and W Kolhörster [6] were the first to use the vertical telescope of Geiger–Müller gas-discharge counters, while L V Mysovskii [7] laid the foundation for the employment of nuclear photoemulsions. The use of an ionization calorimeter in cosmic ray research was for the first time proposed by N L Grigorov, V S Murzin, and I D Rapoport [8] in 1957.

Because the number of particles in nuclear-active (protons, antiprotons, nuclei, antinuclei) and soft (electrons, positrons) components of cosmic rays increases with altitude above sea level, researchers have sought from the very beginning to lift their instruments as high as possible. The surest way proved to place them on balloons and artificial earth satellites (AESs). However, the size and weight of balloon- and satellite-borne equipment are limited.

This paper reviews data obtained in the past 20 years, when high-altitude balloon and AES experiments on the cosmic-ray physics have been conducted with the use of such devices as calorimeters [9, 10], scintillation detectors [11], Cherenkov detectors [12–14], transition radiation detectors [15–18], and magnetic spectrometers [19–21], or their combinations.

Experiments using instruments of each of these types are, as a rule, designed to resolve several physical problems at a time, with different detectors combined in a single device performing similar functions to interchange with and supplement each other. Almost all the above detectors are suitable both to identify particles and to measure their energy. This remark fully refers to calorimeters. However, calorimeters have advantages over other types of detectors for cosmic-ray balloon and satellite experiments. Despite their relatively small size and weight, calorimeters make possible precision measurements. They are also the most reliable systems for long-term autonomous operation. Moreover, there are practically no alternative instruments for the measurement of particle energies above several hundred GeV, the working range of other detectors, for example, magnetic spectrometers, being strongly limited. For these reasons, calorimeters find wide application in cosmic-ray balloon and AES experiments.

A calorimeter, as a rule, constitutes constructionally a module consisting of an absorbing material and detectors, which is crossed by an incident particle. The particle loses energy when passing through the absorber in various processes (electromagnetic or nuclear) and thereby gives rise to secondary particles. The released energy is recorded by the detectors which generate a signal in proportion to the energy of the primary particle. It is this proportionality that makes possible calorimetric measurements of energy.

Calorimeters are used to simultaneously measure the direction and the angle of incidence of particles. As mentioned above, they can also identify particles, distinguishing between protons, nuclei, and electrons [22].

Primary cosmic radiation consists largely of protons and helium nuclei, whereas its leptonic component accounts for only $10^{-2}-10^{-3}$ of the total particle flux, with positrons making up around 10^{-1} of lepton emission. Therefore, the main problem encountered in studies of electron–positron flows is to suppress the proton background. It should be emphasized that measurements with magnetic spectrometers that allow the sign of the particle's charge to be determined require a higher degree of proton suppression than is necessary for the measurement of the integral electron–positron flux. This observation can be accounted for by the fact that a magnetic spectrometer identifies electrons from the sign of the particle's charge against a background of a small number of antiprotons, the fraction of which in the total cosmic ray flux does not exceed $10^{-4}-10^{-5}$. Positrons can be reliably distinguished from background protons if the rejection coefficient (proton-to-electron detection efficiency ratio) is not lower than 10^5.

There are many methods to separate electrons (positrons) from hadrons in a calorimeter, based on the difference between processes accompanying hadron–electron (positron) interactions in the absorbing material [23].

Development of an electron-initiated shower in the substance is phenomenologically described in terms of well-known mechanisms. When the energy of electrons is higher than the so-called critical energy (which depends on the charge of the absorber with which the electrons interact), the major losses are due to electron bremsstrahlung. The resulting photons give rise to electron–positron pairs. Secondary particles, in turn, produce new particles by the same mechanism. Collectively, these processes result in an electromagnetic cascade of particles in the substance [24].

A cascade can just as well develop in the hadron–substance interaction, even if with a smaller probability. A proton-initiated shower develops similarly to an electromagnetic one; the two processes differ only in that the loss of proton energy in matter largely occurs through strong interactions. Around half of the primary particle energy in a nuclear cascade is carried away by the so-called leading particle, and the remaining half is associated with other secondary particles [25]. Strong interactions give rise to relativistic hadrons (mostly pions), nuclei from nuclear decay and/or evaporation, fragments of nuclear fission and scattering. A substantial part of the secondary particles born in a nuclear cascade comprises neutral pions that decompose into γ-quanta and give rise to electromagnetic showers in the substance [26].

In what follows, we discuss methods used in some well-known high-altitude balloon and AES cosmophysical experiments aimed at measuring the composition and energy spectrum of cosmic rays.

2. Instruments and methods used in balloon and satellite cosmophysical experiments

FGST/LAT (formerly GLAST/LAT) (*Fermi Gamma-Ray Space Telescope/Large Area Telescope*) — a telescope for cosmic gamma-radiation research [27] — was launched into Earth's orbit in June 2008. FGST is designed to study cosmic sources of gamma radiation, such as active galactic nuclei, black holes, neutron stars, pulsars, and other high-energy sources, and to search for various manifestations of dark matter. Moreover, FGST has the capacity of registering high-energy electrons in cosmic rays in an energy range of up to 300 GeV (there is a possibility to extend it to 1 TeV) [28].

FGST, shown in Fig. 1a, consists of 16 identical vertical modules, each containing a position-sensitive tracker with 18 silicon strips alternating with absorbing tungsten layers (the main task of the tracker is to measure the direction of incoming gamma-quanta) and a CsI(Tl) calorimeter for precise detection of high-energy electrons and gamma-quanta with a 5–10% resolution in an energy range from 10 to 300 GeV [29]. The instrument is surrounded by 89 scintillation detectors forming an anticoincidence system.

The CsI(Tl) calorimeter (364 mm wide and 224.3 mm high) (Fig. 1b) consists of 8 layers, each containing 12 logs of caesium–iodide crystal stacked in a criss-cross pattern in the adjacent layers. The total thickness of the calorimeter is 8.5 radiation lengths. Such a structure permits observing

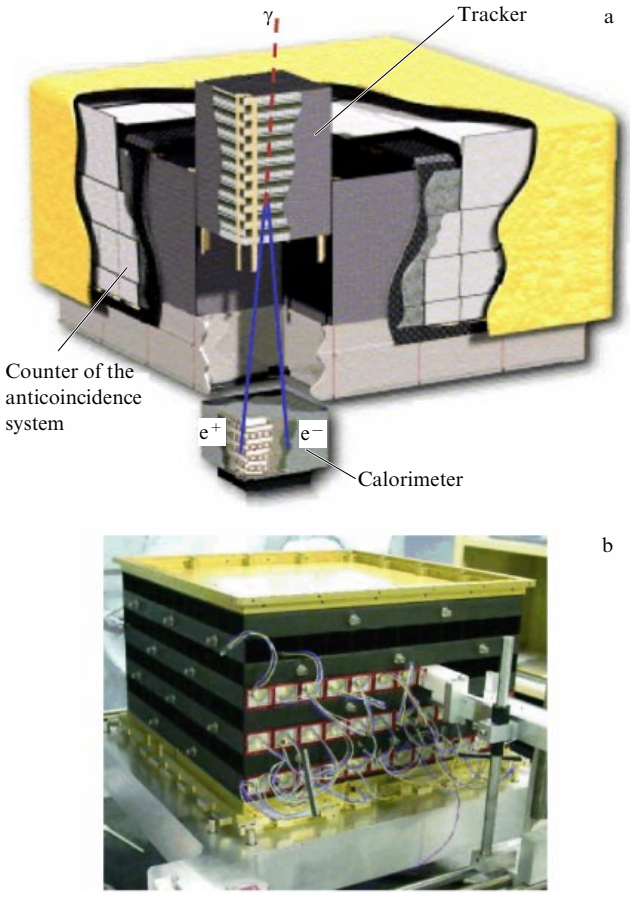

Figure 1. (a) General view of FGST. Incident electrons and γ-quanta interact with the material in the tracker and induce an electromagnetic shower in the calorimeter. (b) General view of the FGST calorimeter.

Table 1.

Criteria	Fraction of selected electrons	Fraction of other selected charged particles	Electron-to-proton selection efficiency ratio
1	0.74	0.25	2.96
1+2	0.60	0.021	28.6
1+2+3	0.55	0.011	50.0
1+2+3+4	0.52	0.0074	70.3
1+2+3+4+5	0.29	0.00025	1160

shower development in space and determining the direction of arrival of particles [30, 31].

Electron–proton separation was achieved practically with the help of the calorimeter alone. The main idea behind this and other electron–positron separation calorimetric experiments consists of estimating the difference in the development of hadronic and electromagnetic cascades in matter.

The following criteria of event rejection were used in selecting electrons in the calorimeter:

(1) Events with energy release below 10 GeV. In this case, particles pass across the entire instrument without interaction or with interaction deep in the calorimeter, which is characteristic of hadrons.

(2) Events with a wide spatial distribution of actuated crystals in the calorimeter. Lepton-initiated showers are much more compact than most hadron-initiated showers (Fig. 2a).

(3) Events with a large number of counter operations in the anticoincidence system, which correspond to a proton transit through the device with large probability (Fig. 2b).

(4) Events with highly asymmetric showers. Electromagnetic showers are much more symmetric than hadronic ones (Fig. 2c).

(5) Events with a shower induced prior to entering the calorimeter. About 90% of the protons remaining after selection based on the above four criteria initiate a shower in the tracker before entering the calorimeter; however, up to 40% of the electrons are also dropped out using this criterion (Fig. 2d).

Table 1 illustrates the efficiency of selection criteria 1–5 for electrons and protons and the relationship between the efficiencies of electron and proton selection that characterizes proton rejection [32].

The calorimeter thickness being small, additional criteria are needed to improve resolution in the high-energy range ($\geqslant$ 100 GeV); they are related to the topology of developing electromagnetic showers and do not influence the efficiency of electron selection and proton rejection.

To sum up, this technique ensures rather high efficiency of electron selection and fairly good efficiency of proton rejection sufficient to experimentally examine electron spectra in the energy range up to hundreds of GeV.

HEAT (*High-Energy Antimatter Telescope*) — an instrument based on a superconducting magnetic spectrometer for research in cosmic ray astrophysics. These studies include

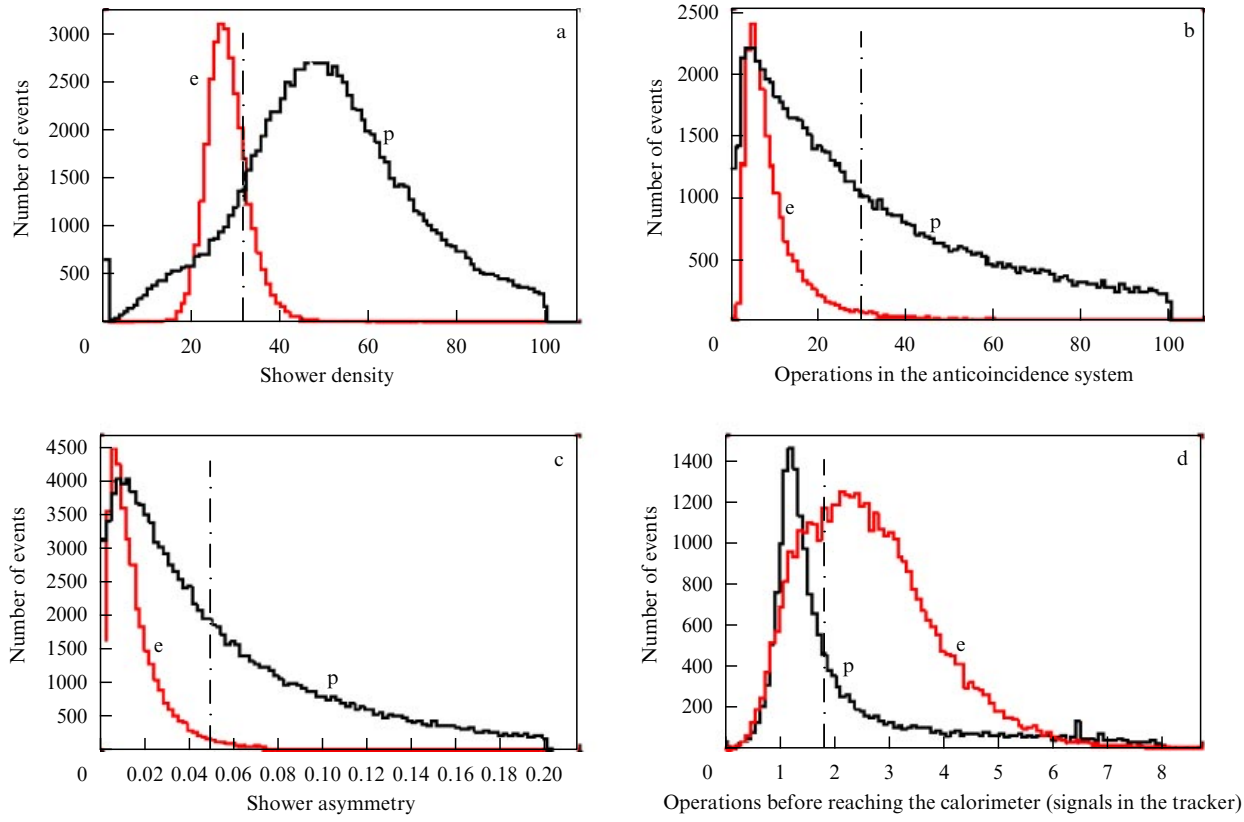

Figure 2. Criteria for the selection of events in the FGST experiment.

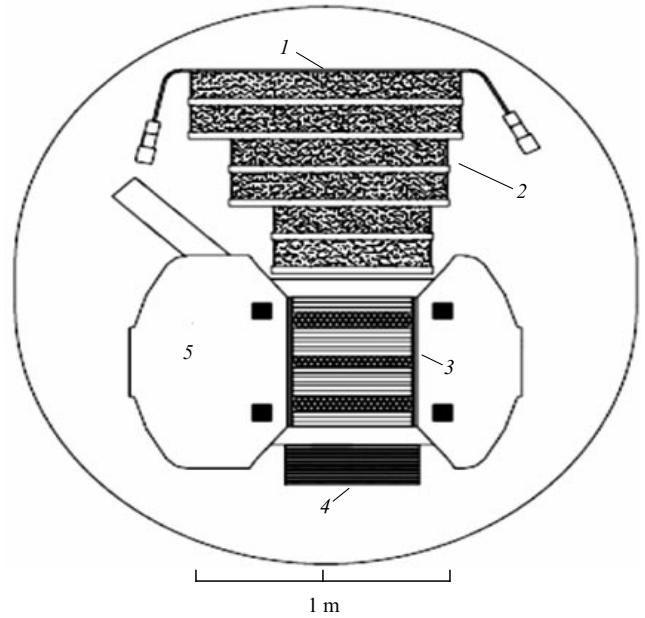

Figure 3. General view of HEAT.

measurement of the relative content and energy spectra of antiprotons, cosmic-ray nuclear isotopes, electrons, and positrons with energies up to 100 GeV.

HEAT (its general view is displayed in Fig. 3) consists of a superconducting magnet *5*, a drift hodoscope *3* combined with a transition radiation detector (TRD) *2*, an electromagnetic calorimeter *4*, and a time-of-flight scintillation system *1*. The instrument was used in two balloon flights in 1994 and 1995 [33].

The hodoscope placed in a magnetic field serves to measure the hardness (momentum divided by particle charge) of particles that fly through it. The hodoscope contains 479 thin-wall drift tubes. Part of them, arranged in 19 layers and having axes parallel to the magnetic field lines, serves to measure the hardness of the traversing particles. The remaining tubes make up 8 layers and have axes orthogonal to the magnetic field lines (these layers provide information necessary to reconstruct particle trajectories in the instrument). Each layer ensures spatial resolution at the level of 70 μm. The transition radiation detector identifies electrons by selectively recording transition radiation from particles with a high Lorentz factor (over 10^3). The time-of-flight system comprises a plane surface with four plastic scintillators on top of the instrument and the first three layers of the electromagnetic calorimeter. The upper scintillators also measure ionization losses of a particle and thereby permit determining its charge.

The calorimeter of HEAT is made of ten modules, each measuring 50×50 cm and containing a 0.5-cm-thick lead plate and a centimeter-thick plastic scintillator layer enveloped by a 0.5-mm aluminium foil to enhance the efficiency of light collection from the scintillators. The overall thickness of the calorimeter amounts to 9.5 radiation lengths. It is suitable for measuring only the longitudinal shower profile (positional measurements are made only along coordinate z), but in the HEAT experiment this device was used to perform a variety of other functions, including measurements of electron energy, hadron rejection, and time-of-flight parameters.

The HEAT geometric factor was 495 cm^2 sr, and the total measurement time ranged 30 hours [34].

Distinguishing electrons against the proton background, it was possible to reach with the aid of TRD the efficiency of electron selection equal to 88% and the efficiency of proton selection at a level of only 0.59%, thus reaching the rejection coefficient close to 170 [35].

However, this was clearly insufficient, taking into account the electron-to-proton flux ratio in cosmic radiation (roughly 1:100 at an energy of up to 100 GeV). Other detectors of HEAT were also used to increase the rejection coefficient and thereby reduce the number of protons simulating electrons and positrons.

One of the methods of electron (positron)–proton separation was based on the difference between distributions of the ratio of energy E measured in the electromagnetic calorimeter to momentum p obtained in the drift hodoscope. This distribution for electrons and positrons shows a peak at the E/pc ratio of -1 and $+1$, respectively. The peak of distribution for protons occurs at E/pc ratio equal to $+0.5$ because a large fraction of energy released in the calorimeter during the passage of protons escapes from it [36].

Moreover, the calorimeter can by itself reduce the proton background in two more ways. First, analog signals from its seven lower layers are summed to roughly yield the total energy release from a shower. Because one of the conditions for trigger operation includes the requirement that the total amplitude exceeds a certain level (0.5 GeV), by setting this level we reject protons with higher penetrating power. This method is analogous to the one used in the FGST experiment and considered in the preceding section; it selects events by taking into account total energy release in the calorimeter.

The second method makes use of the fact that interacting protons generate in the calorimeter cascades of different sizes with characteristics distinct, as a rule, from those of electromagnetic cascades. Specifically, they possess a higher value of the χ^2 goodness-of-fit test, when the longitudinal profile of a hadronic shower is approximated by the mean cascade curve of an electromagnetic shower. The distribution of electron and proton events in terms of this parameter is shown in Fig. 4a. The dependence of proton selection efficiency on that of electrons when varying the threshold selection value in χ^2 from 1 to 2 is illustrated in Fig. 4b.

It can be seen from Fig. 4b that the highest ratio of electron selection efficiency to proton rejection can be achieved by choosing threshold χ^2 values corresponding to electron and proton selection efficiencies of $\sim 90\%$ and $\sim 10^{-3} - 10^{-2}$, respectively. In addition, the minimal energy release threshold should be established simultaneously, because noninteracting protons releasing little energy and low-energy electrons produce weak showers in a calorimeter with great layer-to-layer energy release fluctuations. This means that large fluctuations and poor measurement accuracy of the released energy (because in this case its values fall within the starting section of the working range for energy releases measured by a scintillator) are responsible for a small χ^2 value corresponding to a high-energy electromagnetic cascade.

Thus, the use of methods for suppressing proton events with the aid of a calorimeter and a hodoscope ensures electron selection efficiency at the level of 97% and a rejection coefficient ranging to 460. The combination of this approach and the use of methods based on a transition radiation detector permit obtaining a rejection coefficient

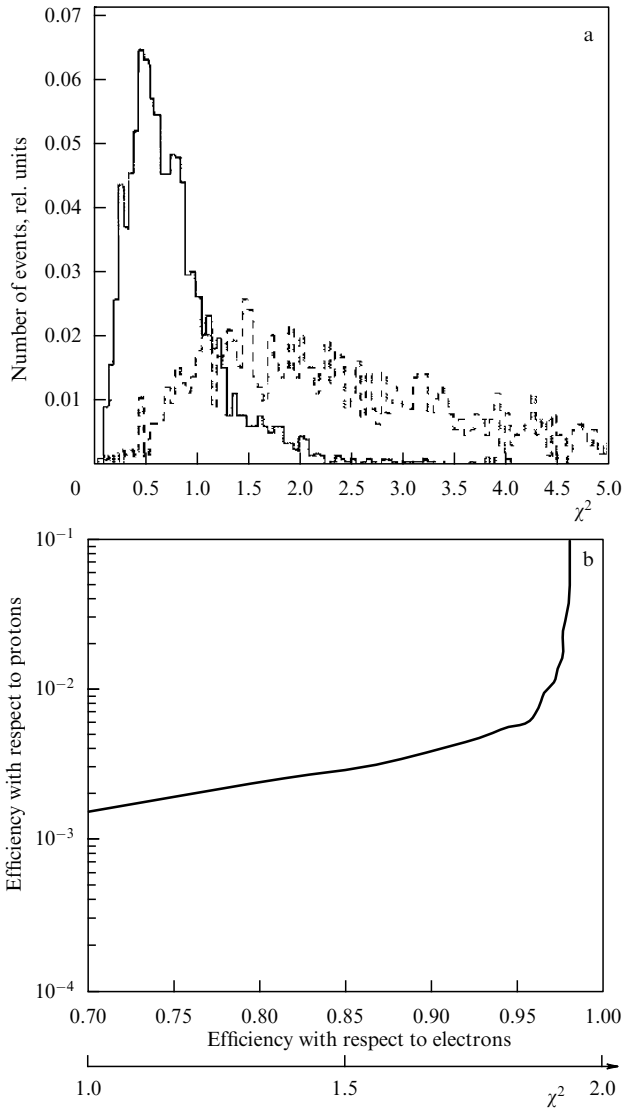

Figure 4. (a) Distributions of χ^2 for electrons (solid curve) and protons (dashed curve). Histogram areas are normalized to unity. (b) Dependences of proton and electron selection efficiencies when varying the threshold selection values in χ^2 from 1 to 2.

on the order of 8000, sufficient for the electron and positron energy range (up to 100 GeV) measured in this experiment [37].

BETS (*Balloon-borne Electron Telescope with Scintillating fibers*) — an experiment to study electron components of cosmic rays in an energy range from 10 GeV to hundreds of GeV in a series of balloon flights (in 1995, 1997, 1998, and 2004); the design of the instruments used during the experiment somewhat varied (a different number of lead layers and plastic scintillators). Described below is the instrument used in the 2004 experiment (Polar Patrol Balloon, PPB). It contained a detector consisting of 36 layers of scintillating fibers having a cross section of 1 mm^2 each, 9 plastic scintillators, and 14 lead plates (the total thickness of the detector amounted to 9 radiation lengths). In other words, the detector functioned as a calorimeter with a 28×28 cm sensitive surface [38]. It is schematically shown in Fig. 5.

Scintillating fibers are arranged at a right angle to one another in two adjacent layers in order to record cascade particles formed in the lead in two projections, x and y.

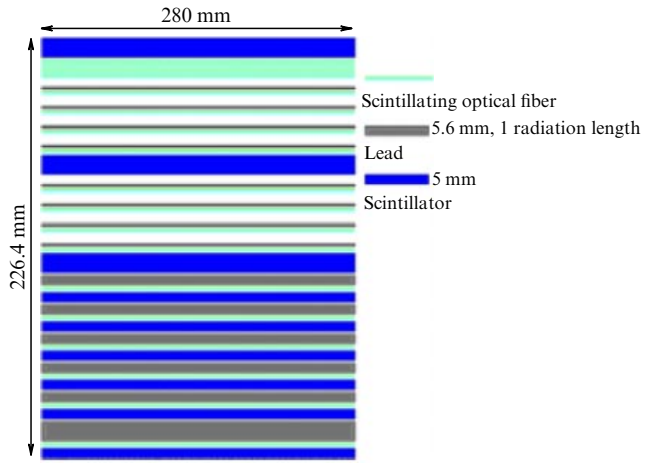

Figure 5. Schematic of BETS.

A scintillation signal in the fibers is read out by a special signal-amplifying ccd (charge-coupled device) camera for each projection x and y. The shower development pattern observed in the ccd camera coordinates was reconstructed from the fiber position in the detector volume [39].

The trigger system of the instrument is organized so as to record only showers originating in the first layers of the calorimeter, which accounts for the 100-fold lower efficiency of proton registering compared with that of electrons. The first layer of the trigger system scintillators is located immediately ahead of the calorimeter, and two others deep inside it. Each scintillator has a specific operation threshold corresponding to the energy release in the shower induced by electrons with an energy of 10 GeV.

In this way, the trigger selects particles that release more energy when passing through the calorimeter than a 10-GeV electron and thereby rejects a large number of protons and helium nuclei that interact only in the lower half of the detector or do not interact at all. The proton rejection coefficient in this selection by a trigger is roughly 100.

In addition, it was important to reconstruct the shower axis for electron selection in this experiment, as described below. First, the center of gravity of energy release is found in the shower development cross section in each fiber layer at a depth of more than 3 radiation lengths in the instrument. These points are used to restore the cascade axis by the least-square technique. Second, the position of the center of gravity of energy release in the shower is determined in each layer, taking account only of signals from the fibers close to the shower reconstructed axis (not more than 5 fibers apart). In this way, reconstruction of the shower axis is repeated from the refined positions of the centers of gravity. As a result, the axis position error is not more than 1° [40].

The characteristic transverse size of an electromagnetic shower in lead is on the order of 3 cm (the Mollier radius for lead is roughly 1.6 cm), and proton-initiated showers undergo a wider transverse spread due to the generation of pions in nuclear interactions. Electron- and proton-like events reconstructed from the balloon flight data are shown in Fig. 6. Electrons were selected using simulation.

Distributions over E_r (ratio of energy release in a cylinder with a radius of 5 mm and the axis formed by the shower axis to the total energy release in the calorimeter) were constructed for simulated electron and proton events; they are presented in Fig. 7.

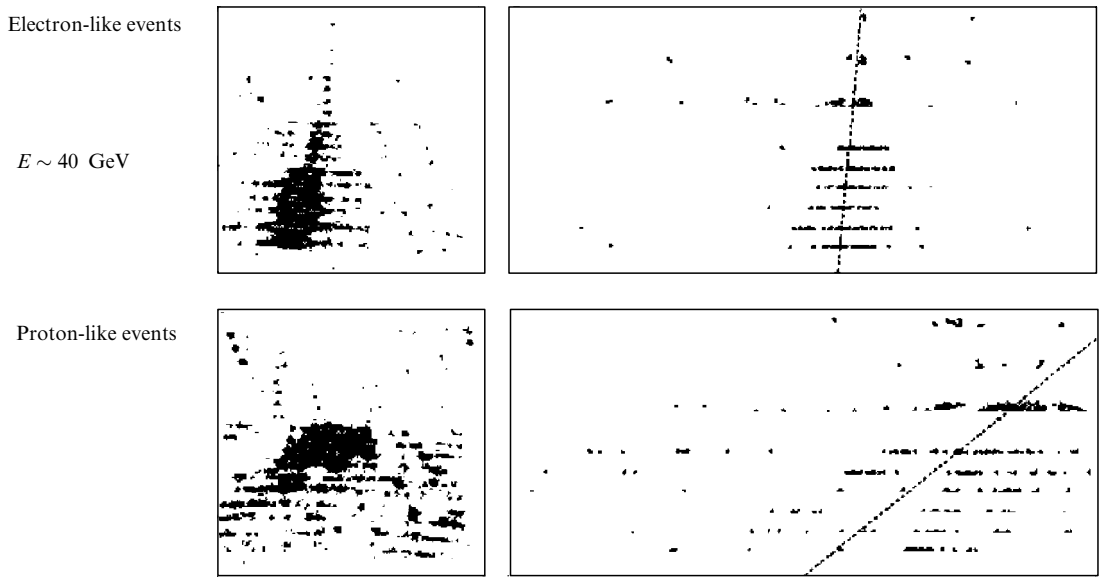

Figure 6. Examples of restored events in the BETS calorimeter.

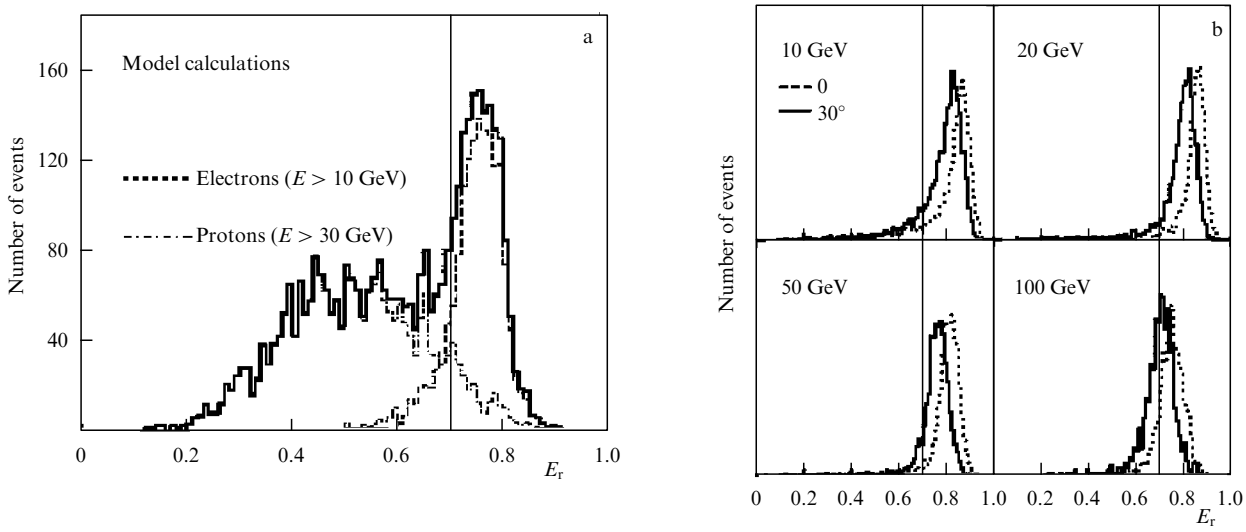

Figure 7. (a) Distribution of events over E_r values. (b) Distribution of events over parameter E_r at different energies and angles of incidence of electron-induced showers upon the instrument in the CERN accelerator test experiment.

The results of the simulation were also verified by an accelerator test experiment at different angles of incidence of the particles upon an instrument. Figure 7b illustrates E_r distribution for electrons at the angles of incidence equal to 0 and 30°.

The theoretical distribution of events in terms of E_r values is in good agreement with that in the accelerator experiment. As follows from Fig. 8 showing energy dependences of the efficiency of electron and proton selection, the former is practically independent of the electron incidence angle.

An evaluation of the probability of protons passing through such a selection procedure shows that it strongly depends on the angle of incidence; it is estimated at 10% for vertically falling particles, and at a few percent for an angle of incidence equal to 30°. The energy dependence of the probability of electron and proton selection at several fixed angles of incidence is illustrated in Fig. 8. The mean energy of the proton-induced cascade being roughly 3 times lower than that of the electron-induced cascade at the same particle's

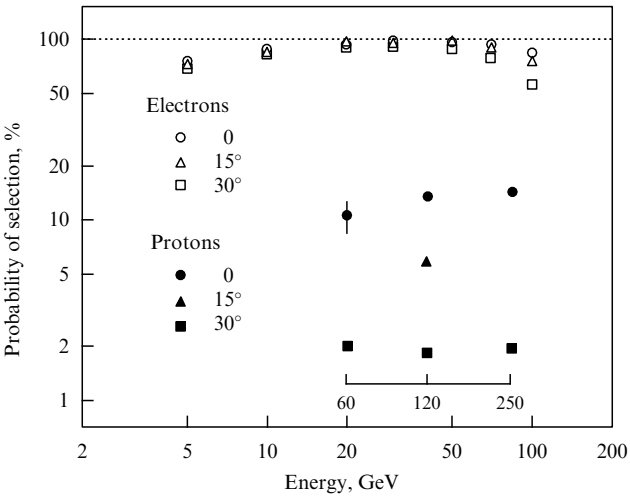

Figure 8. Efficiency of electron and proton selection by parameter E_r at different primary energies, derived from the results of the accelerator test experiment.

primary energy, the energy scale for protons in the figure was changed threefold [41].

The rejection coefficient for protons during selection by E_r turned out to be 20. Combining this criterion for electron selection with the criterion for trigger operation yields a rejection coefficient on the order of 2000, quite sufficient for electron selection in the BETS energy range up to several hundred GeV.

PAMELA (*a Payload for Antimatter–Matter Exploration and Light–nuclei Astrophysics*) — an experiment aboard the Resurs-DK1 satellite launched into Earth's orbit in June 2006. It is designed to study the composition and energy spectra of cosmic particles in near-Earth space. The apparatus comprises a calorimeter, a magnetic microstrip spectrometer, a time-of-flight scintillation system, anticoincidence detectors, a scintillation shower detector, and a neutron detector. Schematic drawing of the apparatus is shown in Fig. 9 [42].

Most criteria for electron–proton separation in the PAMELA experiment are based on the use of a calorimeter.

The discrete calorimeter (Fig. 10) consists of 44 sensitive silicon planes 380 μm in thickness alternating with tungsten-based plane absorbing layers. Total calorimeter thickness amounts to 16.3 radiation lengths or 0.6 nuclear lengths. Each of the 44 sensitive planes consists of 9 silicon detectors divided in turn into 32 strips. Strips in successive layers are arranged mutually perpendicular to record shower development in two projections [43].

As mentioned earlier, reconstruction of the shower axis in the calorimeter is important for the separation of electrons (positrons) from protons. In the PAMELA experiment, where it is possible, the axis of the cascade (corresponding to the primary particle trajectory) is found with the help of the magnetic spectrometer, otherwise the axis is determined using a calorimeter. Because the 44 silicon-based planes are divided

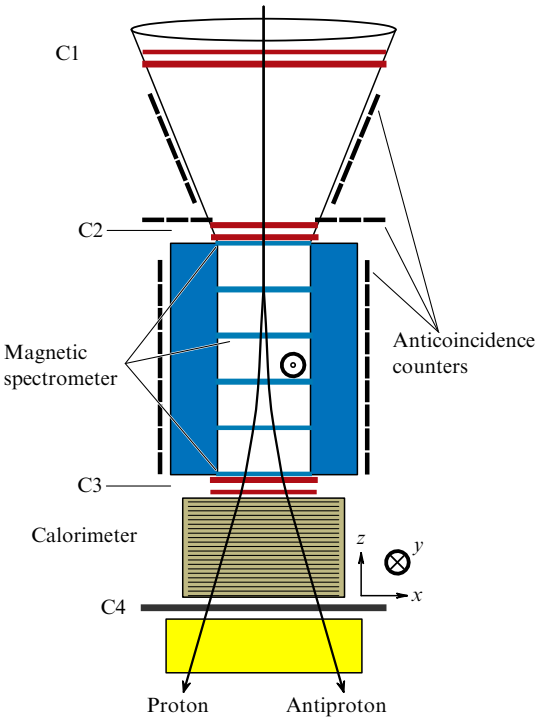

Figure 9. Physical scheme of the PAMELA apparatus. C1–C4 are the scintillators.

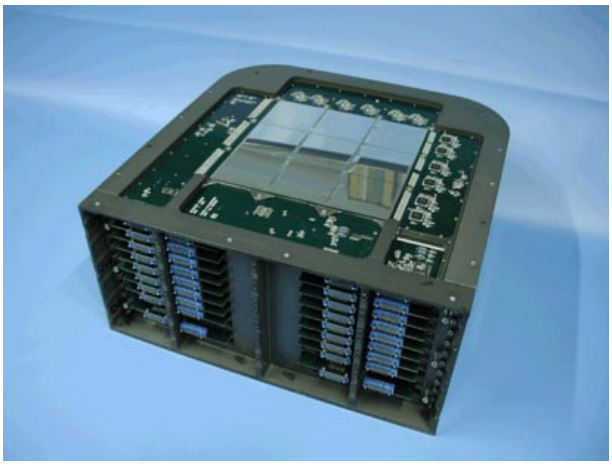

Figure 10. General view of the PAMELA calorimeter.

into strips, the trajectory of particle i intersects a plane in the center of gravity $\bar{x}$ of measured energies E_i (> 0.7 mip) released in the strips with coordinates x_i, where

$$\bar{x} = \frac{\sum_i x_i E_i}{\sum_i E_i} .$$

(1 mip corresponds to the energy released during passage of a minimum ionizing particle.)

When this procedure is performed for a few layers in the calorimeter, the shower axis can be found by the least-square technique. The axis position error is on the order of one degree [44].

The first and most efficacious criterion for the selection of electrons against the background of protons is comparison of momentum measured with the magnetic spectrometer and energy measured with the calorimeter. Hadrons with a given energy are characterized by a flat distribution of the total energy release with a peak corresponding to its low level (from noninteracting protons), whereas for electrons, the distribution is normal. However, the tail of the distribution for high-energy electrons in the low energy release region may reduce the efficiency of selection. Figure 11 displays distributions of total energy release for 50-GeV protons and electrons. Almost 99.98% of the protons and only 4.3% of the electrons are rejected after the selection of events at this energy with an energy release of over 7000 mip.

Another feasible criterion for electron–proton separation in the PAMELA experiment involves selection by the onset of a shower in the calorimeter, the probability of development of an electromagnetic shower in the first three planes being 89%. For hadron cascades, starting points of shower are uniformly distributed over the entire calorimeter length due to its small thickness (0.6 nuclear lengths).

The critical aspect of this method is the necessity of pinpointing the location of the shower development origin.

Quantity

$$R = \sum_{j=1}^{2} \sum_{i=1}^{pl_{\max}} n_{ij}\, i$$

reflects topological characteristics of shower development in the calorimeter. Secondary particles in a shower being collimated along its axis, this quantity is related to the

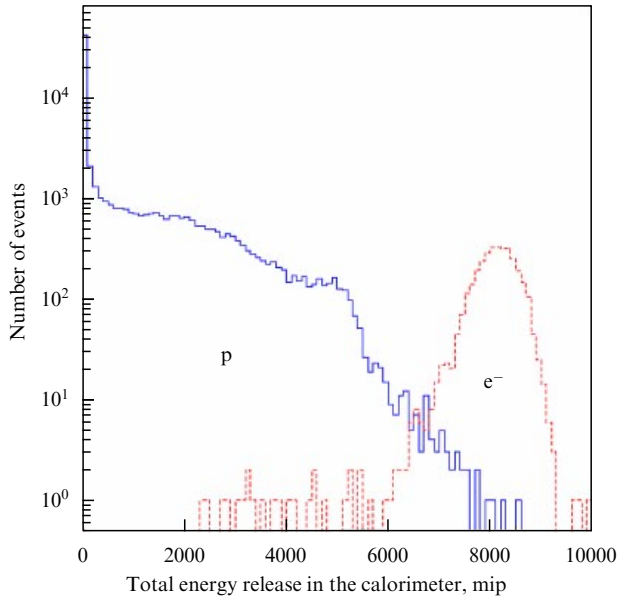

Figure 11. Distribution of total energy release in the calorimeter over the number of events for 50-GeV protons and electrons.

starting point of shower. It is defined as the sum of strip operations n over calorimeter planes at a distance of two Mollier radii from the reconstructed shower axis. Summation over planes is performed up to the plane with a number pl_{max}, corresponding to the position of the shower maximum in the calorimeter at a given initial energy. This value can be derived either from magnetic spectrometer data or from results of the accelerator test experiment. The values of R are higher for electromagnetic showers than for most noninteracting or partially interacting hadrons. Figure 12 depicts the distribution over quantity R for simulated 100-GeV electrons and protons [45].

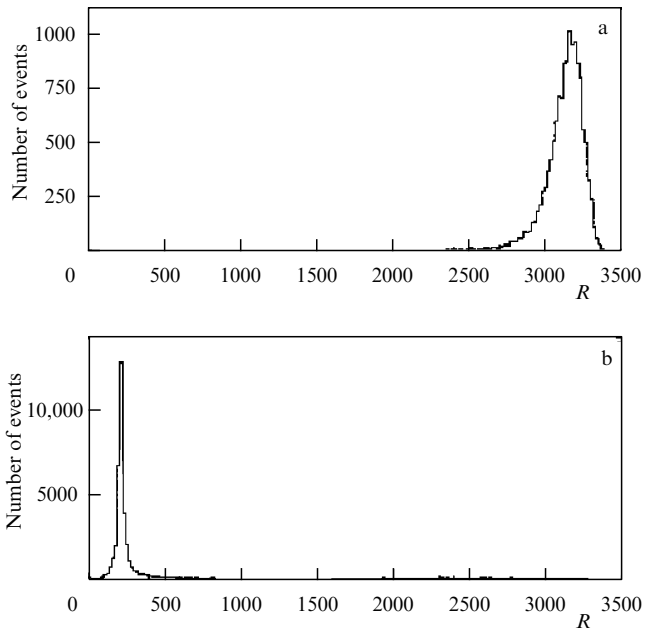

Figure 12. Distribution over quantity R for 100-GeV electrons (a) and protons (b).

The distance of two Mollier radii is chosen on the assumption that an electromagnetic cascade in a cylinder of such radius releases over 95% of its energy, i.e., much more than a hadronic one. Moreover, the distance of two Mollier radii is optimal, as shown in the course of CAPRICE (Cosmic AntiParticle Ring Imaging Cherenkov Experiment) [46, 47].

The energy released from an electromagnetic shower sharply decreases after it passes through the maximum. The position of the maximum in the PAMELA experiment is found from the particle momentum measured by the magnetic spectrometer or in the beam test experiment. The energy of hadron showers is distributed more or less uniformly and the maximum of the development of any hadron cascade in the calorimeter lies deeper than that of an electromagnetic one at the same initial energy. The shower longitudinal profile can be characterized by determining the fraction of total energy released in the next five layers after the one where the shower maximum is expected. Another way is to estimate the amount of energy released in the last four layers of the calorimeter within a cylinder with a radius equivalent to two Mollier radii. Moreover, particle identification is possible based on the amount of energy released in individual strips. For hadron showers, it could be very high due to fragmentation of silicon nuclei [48].

Most parameters used in different methods were preliminarily optimized by Monte Carlo simulation.

Thus, PAMELA employs a combination of the above methods for electron–proton separation and thereby yields a proton rejection coefficient of 10^5 for energies in excess of 10 GeV, and 90% efficiency of electron selection. However, at particle energies of several hundred GeV, the magnetic spectrometer measures hardness with a low accuracy. In this case, separation of protons based on the comparison of momentum measured with a magnetic spectrometer and energy measured with a calorimeter is impracticable. The employment of the calorimeter alone (without trackers) gives a rejection coefficient of 10^4 at energies of up to a few hundred GeV [49], which is quite sufficient for measuring the total electron/positron flux in this energy range.

ATIC (*Advanced Thin Ionization Calorimeter*) — an experiment designed to study the composition and energy spectra of high-energy cosmic particles. A few long-lasting balloon flights were undertaken from December 2000 to January 2001, from December 2002 to January 2003, and from December 2007 to January 2008. A diagrammatic sketch of the apparatus is presented in Fig. 13. It consists of a silicon matrix to measure a charge of particles passing through it, a graphite target (0.75 nuclear lengths) where particles interact, three layers of scintillation detectors to initiate a trigger and detect the particle's trajectory, and a calorimeter identifying particles and measuring their energy.

The calorimeter (Fig. 14) is made from bismuth germanate (BGO) crystals and has a thickness of 18 radiation lengths. The calorimeter is divided into ten 50×50 cm layers each containing 40 BGO crystal bars measuring $2.5 \times 2.5 \times 2.5$ cm. The bars in adjacent layers are arranged mutually perpendicular to measure the spatial distribution of particles in a shower and to determine its axis [50].

ATIC is guided by the following set of criteria for separating electrons from protons.

First, the characteristics of mean electron shower curves were provided by simulation. It was found that electrons and protons lose up to 97 and only 40% of their energy in BGO

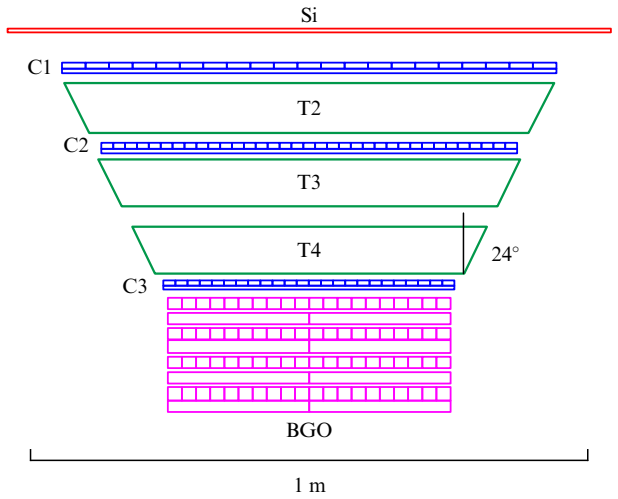

Figure 13. Schematic drawing of ATIC.

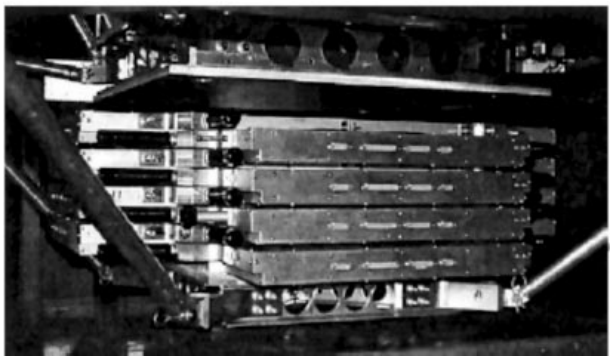

Figure 14. General view of the ATIC calorimeter.

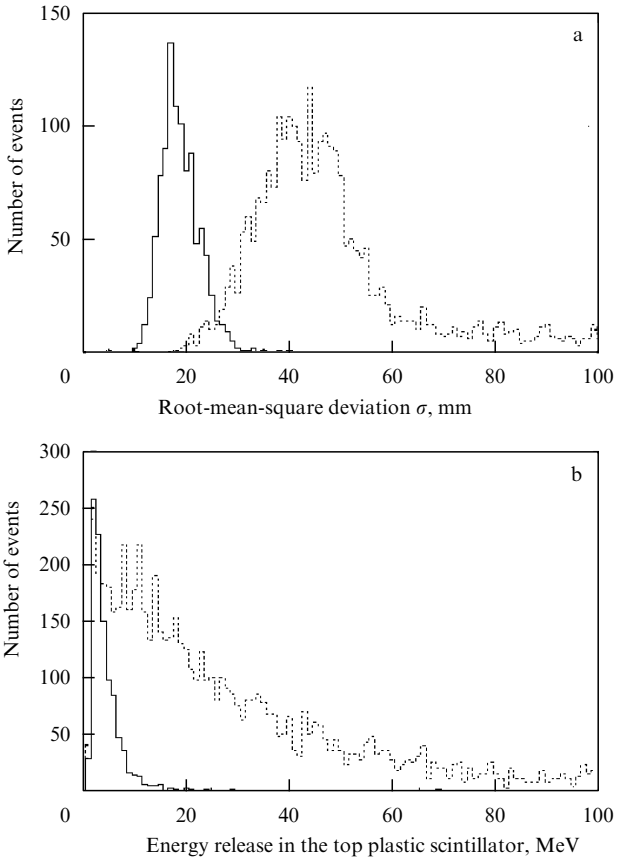

Figure 15. (a) Distribution of electron (solid curve) and proton (dotted curve) events by root-mean-square deviations of energy release distributions in the first plane of the calorimeter. (b) Energy release distribution for electrons (solid curve) and protons (dotted curve) in the top plastic scintillator.

crystals, respectively. Cascade longitudinal profiles were approximated by shower curves obtained from simulations for electrons. The requirement of good approximation was dictated by the value of χ^2. This method is similar to the one used in the HEAT experiment, where approximation of the longitudinal shower profile by the curve for the electromagnetic cascade was also followed by computation of χ^2. Based on this criterion, some 5% of the electrons were rejected and about 68% of the protons suppressed.

Second, transverse particle distribution in the shower was utilized. In particular, the upper layers of the calorimeter demonstrate high efficiency of electron–proton separation due to the fact that fluctuations at the early stages of the development of hadron-initiated showers are greater than for electron-induced ones. Figure 15 illustrates the root-mean-square (standard) deviations of energy release distributions in the first plane. The same parameter for individual planes is calculated as follows:

$$\sigma^2 = \frac{\sum_{i=1}^{n} E_i (x_i - x_c)^2}{\sum_i^n E_i} ,$$

where x_c is the coordinate of the center of gravity of energy release, x_i is the coordinate of the i-th crystal center, and E_i is the energy release in the i-th crystal. Summation is taken over all crystals of a given layer [51].

Third, the backscattering, which differs for hadronic and electromagnetic showers, was considered. The number of secondary particles passing backward away from protons is significantly higher than that from electrons. Plastic scintillators alternating with the target can measure their number for each event. Simultaneously, differences in the types and fluxes of backscattered particles may be used. In proton events, backscattered particles usually yield high energy deposition in comparison with the electron events mostly producing low-energy γ-quanta that usually release no more than 2 MeV of energy per event. Penetrating charged particles release more energy than that. Figure 15b shows the difference in energy release distributions in the top plastic scintillator for electrons and protons that collectively liberate roughly 1 TeV of energy in the calorimeter.

Although the transverse electron and proton shower profiles become more and more different with increasing depth, one more parameter was introduced to improve electron–proton separation. Figure 16 represents the distribution of events in terms of energy release dispersion in individual bismuth germanate layers, and the fraction of energy released in the n-th layer (the ratio of energy release E_n to the total energy release E_{sum} in the calorimeter). The abscissa axis shows root-mean-square deviations of energy releases from the center of gravity of energy release in a given layer.

The best criterion for electron–proton separation in the first layer of BGO crystals is shower width. Two distributions of width values (for electrons and protons) in the fifth layer partly coincide but become distinguishable closer to the lower layer of the calorimeter. However, an employment of a single criterion, for instance, shower width or energy release, is no

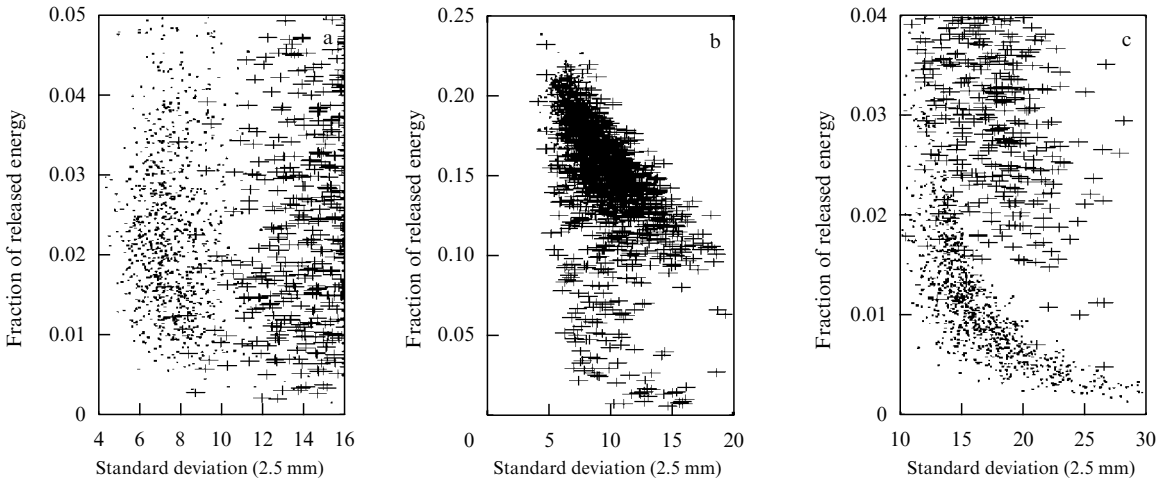

Figure 16. Scatter diagrams of energy release for individual events at three different depths of the calorimeter: (a) in a first layer, (b) in a fifth layer, and (c) in a tenth layer.

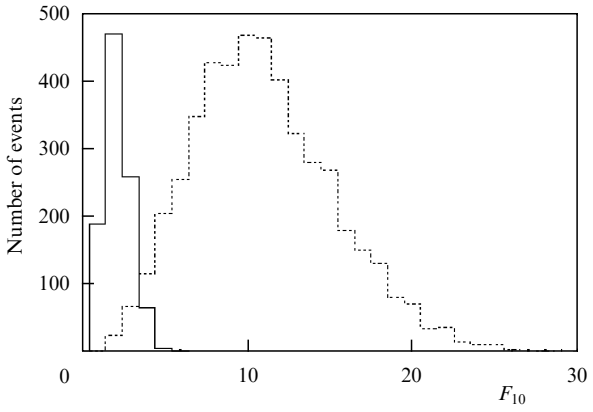

Figure 17. Distributions of electrons (solid curve) and protons (dotted curve) over parameter F_{10} in the last (tenth) BGO layer of the calorimeter.

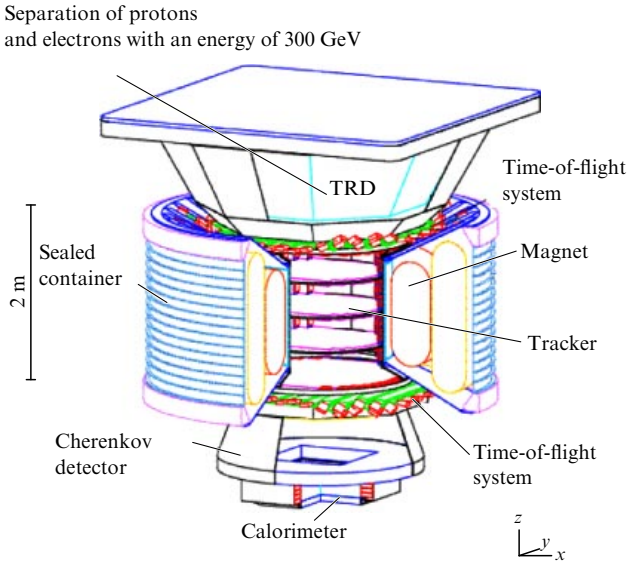

Figure 18. General view of the AMS-02 apparatus.

longer sufficient for the desired separation. Because of this, a special function was selected to take into account these criteria all at once: $F_n = (E_n/E_{\text{sum}})\,\sigma^2$, where σ is the root-mean-square deviation. This empirical function has a rather simple form. Plotting the distributions of function F_{10} in a BGO crystal layer for electrons and protons (Fig. 17) provide two distributions showing as good a separation of these particles as in Fig. 15a. In other words, up to 99% of the proton events can be rejected.

Consideration of all above criteria used in the ATIC experiment ensures approximately 70% efficiency of electron selection and rejection of all but 0.05% of the protons. To recall, a similar total release of energy from protons and electrons in the calorimeter, but not their primary energy, is meant in all cases. Also, a rather high efficiency of electron selection and proton rejection was achieved despite the fact that neither the design nor the components of the instrument as a whole were specially intended for the measurement of electron energy spectra [52].

AMS-02 (*Alpha Magnetic Spectrometer*) — an instrument designed to take measurements aboard the International Space Station, including the composition and spectra of charged cosmic rays in an energy range of up to several TeV and energy of γ-quanta in an energy range of up to several hundred GeV. The previous modification of the instrument, AMS-01, was operated aboard the *Discovery* shuttle for 10 days in 1998. AMS-02 shown in Fig. 18 [53] contains a transition radiation detector (TRD), time-of-flight system of plastic scintillators, tracker consisting of 6 layers of silicon microstrip detectors, superconducting magnet surrounding the tracker, Cherenkov detector, and electromagnetic calorimeter [54].

The calorimeter is shaped like a 17-cm-high parallelepiped with a 65×65 cm^2 base divided into 9 large layers oriented mutually perpendicular to make measurements along coordinates x and y. Each large layer is in turn divided into 11 layers of 1-mm-thick lead foil alternating with 10 layers of scintillating fibers 1 mm in diameter. The entire assembly is glued with epoxide resin (Fig. 19). The calorimeter thickness amounts to about 15 radiation lengths.

There are several methods to suppress protons in the course of the selection of electrons in the AMS experiment, in which different detectors are used.

The transition radiation detector is capable of separating positrons from protons with a rejection coefficient from 10^3 to 10^4 in an energy range of 1.5–300 GeV.

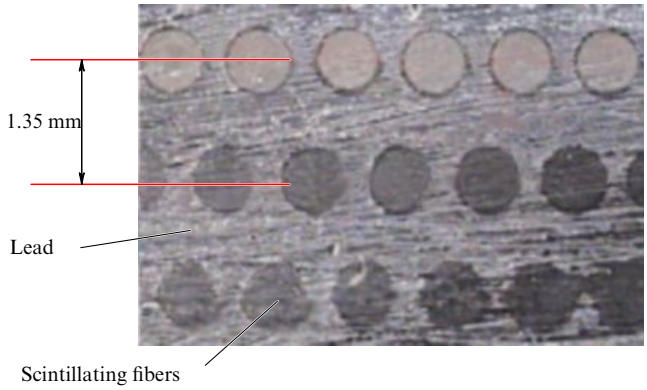

Figure 19. Part of a large layer in the AMS calorimeter.

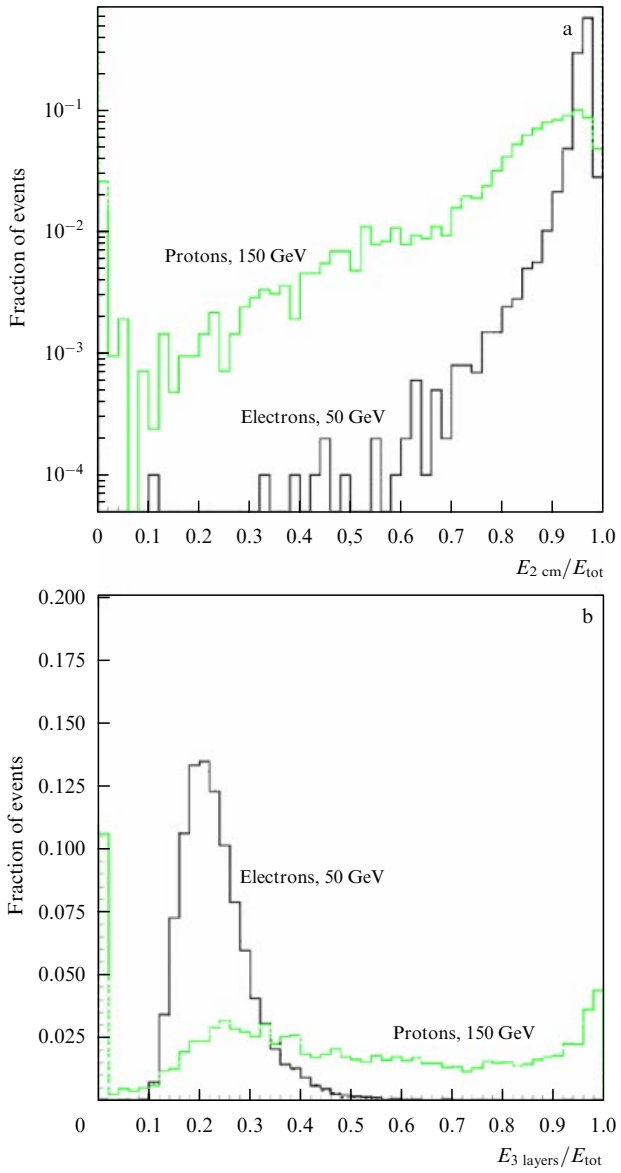

Figure 20. (a) Distribution of energy released in a cylinder with a radius of 2 cm ($E_{2\,\mathrm{cm}}$) along the shower axis in the calorimeter. (b) Distribution of energy released after shower maximum. $E_{3\,\mathrm{layers}}$ — energy released in the last three large layers; E_{tot} — total energy release.

When using only calorimeter in the AMS experiment, the proton rejection coefficient is $\sim 10^4$ in an energy range from 1 GeV to 1 TeV, i.e., a broader one than that accessible for TRD. A rejection coefficient of 10^4 is sufficiently high to select electrons but too low for positron selection in the above energy range. Nevertheless, a combination of these two detectors allows for proton suppression even in the range of up to 300 GeV, with a rejection coefficient of 10^6 being quite sufficient to select positrons [56].

The AMS experiment using calorimeter selects electrons based on such characteristics as the fractions of energy release in a cylinder with a radius of 2 cm along the shower axis and in the last three large layers after the cascade maximum. All these methods were considered in one way or another in the preceding sections.

Figure 20a illustrates the distributions of the ratios of energy release in a cylinder with a radius of 2 cm along the shower axis to the total energy release in the calorimeter for protons and electrons, which were calculated from the results of the accelerator test experiment. The figure shows regions where the ratios (> 0.6) overlap. Figure 20b displays the distributions of the ratios of energy release in the last three large layers to the total energy release, based on the same data. Notice that the overlap region is smaller but the electron distribution has a 'tail' that can reduce selection efficiency.

Nevertheless, efficiency of electron selection in the AMS experiment based on the above criteria amounts to 95% [57].

3. Conclusion

A great variety of detectors for particle identification have been used in recent cosmic-ray balloon and satellite experiments in near-Earth space, viz. the Cherenkov detector, TRD, the magnetic spectrometer, and the calorimeter. A higher rejection coefficient is needed for the selection of positrons than electrons (e.g., 10^5 and 10^3 in an energy range of up to several hundred GeV, respectively). Such a strict proton suppression requires the necessity to combine detectors of different types for the selection of electrons and especially positrons.

At present, the calorimeter is practically a single powerful instrument for proton suppression and precision energy measurements. which is suitable, by virtue of its small size and mass, for reliable long-term operation in balloon and satellite experiments.

Calorimeters can be used not only for the designed purpose of energy measurement but also for particle identification. A variety of calorimeter-based methods for electron–proton separation in cosmic rays were used in the ATIC, AMS-02, FGST, PAMELA, BETS, and HEAT experiments. All of them are based on the difference between processes of hadronic and electromagnetic shower development. The methods described in this paper utilize the characteristics of longitudinal and transverse shower development, such as the backscattering, the total energy release in a calorimeter, and some others.

Most calorimeters used in the above experiments have a rejection coefficient on the order of 10^4. This is sufficient to select electrons but not positrons. Nevertheless, combining a calorimeter with a magnetic spectrometer and TRD permits increasing the proton rejection coefficient to $\sim 10^6$ with an efficiency of electron selection of 80–90%. It should be borne in mind, however, that the upper limit for particle energy measurement in magnetic spectrometers and TRDs is rather

low (a few hundred GeV) compared with that in a calorimeter (10 and about 1000 TeV for electrons and hadrons, respectively) [58, 59].

Doubtless, with further advances in calorimetric technology, calorimeters will remain the most important tools for cosmic-ray balloon- and satellite-borne experiments [60].

References

1. Lezhneva O A *Elektrichestvo* (11) 79 (1956)
2. Wulf T *Phys. Z.* **5** 152 (1910)
3. Hess V F *Phys. Z.* **13** 1084 (1912)
4. Skobeltzin D W *Z. Phys.* **43** 354 (1927)
5. Veksler V I *Usp. Fiz. Nauk* **78** 538 (1962) [*Sov. Phys. Usp.* **5** 1024 (1963)]
6. Bothe W *Z. Phys.* **59** 1 (1929)
7. Mysovskii L V *Usp. Fiz. Nauk* **10** 545 (1930)
8. Grigorov N L, Murzin V S, Rapoport I D *Zh. Eksp. Teor. Fiz.* **34** 506 (1958) [*Sov. Phys. JETP* **7** 348 (1958)]
9. Marrocchesi P S et al. *Nucl. Instrum. Meth. Phys. Res. A* **535** 143 (2004)
10. Bellotti R et al. *Astropart. Phys.* **7** 219 (1997)
11. Seo E S et al. *Adv. Space Res.* **33** 1777 (2004)
12. Boezio M et al. *Astrophys. J.* **532** 653 (2000)
13. Aguilar Benitez M et al. "The ring imaging Cherenkov detector (RICH) of the AMS experiment", in *Proc. of the 29th Intern. Cosmic Ray Conf., Pune* (2005)
14. Bergström D et al., in *Proc. of the 26th Intern. Cosmic Ray Conf., Salt Lake City, UT, USA* Vol. 5 (Eds D Kieda, M Salamon, B Dingys) (1999) OG 4.1.21, p. 80
15. Olzem J et al. "Construction of the AMS-02 transition radiation detector for the International Space Station", in *Proc. of the 29th Intern. Cosmic Ray Conf., Pune* (2005)
16. Wakely S P et al. "Transition radiation detectors for cosmic rays near the knee", in *Proc. of the 28th ICRC, Tsukuba* (2003) p. 2237
17. Maestro P et. al. "Energy cross-calibration from the first CREAM flight: transition radiation detector versus calorimeter", in *Proc. of the 30th ICRC, Merida, México* Vol. 2, OG part 1 (2007) p. 333
18. Seo E S "New observations with CREA", in *Proc. of the 29th Intern. Cosmic Ray Conf., Pune* Vol. 10 (2005) p. 185
19. Golden R L et al. *Astrophys. J. Lett.* **457** L103 (1996)
20. Hof M et al. *Nucl. Instrum. Meth. Phys. Res. A* **454** 180 (2000)
21. Yoshida T et al. *Adv. Space Res.* **33** 1755 (2004)
22. Leroy C, Rancoita P-G *Rep. Prog. Phys.* **63** 505 (2000)
23. Fabjan C W, Gianotti F *Rev. Mod. Phys.* **75** 1243 (2003)
24. Amaldi U *Phys. Scr.* **23** 409 (1981)
25. Wigmans R *Calorimetry: Energy Measurement in Particle Physics* (New York: Oxford Univ. Press, 2000) p. 26
26. Ferbel T (Ed.) *Experimental Techniques in High-Energy Nuclear and Particle Physics* 2nd ed. (Singapore: World Scientific, 1991) p. 274
27. Fermi Gamma-ray Space Telescope (formerly GLAST) Collab., http://fermi.gsfc.nasa.gov/
28. Dubois R "GLAST Large Area Telescope: launched and being commissioned", presented at *ICHEP 2008, Philadelphia, PA, USA*
29. Lott B et al. *Nucl. Instrum. Meth. Phys. Res. A* **560** 395 (2006)
30. Bergenius Gavler S et al. *Nucl. Instrum. Meth. Phys. Res. A* **545** 842 (2005)
31. Johansson G, PhD Thesis (Lund, 2008)
32. Moiseev A, Ormes J F, Moskalenko I, in *Proc. of the 30th Intern. Cosmic Ray Conf., Merida, México, 2007*, OG 1014, p. 2
33. Barwick S W et al. *Astrophys. J. Lett.* **482** L191 (1997)
34. Barwick S W et al., astro-ph/9703192
35. Beatty J J et al. *Phys. Rev. Lett.* **93** 241102 (2004)
36. DuVernois M A et al. *Astrophys. J.* **559** 296 (2001)
37. Barwick S W et al. *Nucl. Instrum. Meth. Phys. Res. A* **400** 34 (1997)
38. Torii S et al. *Adv. Space Res.* **37** 2095 (2006)
39. Torii S et al. *Adv. Polar Upper Atmos. Res.* **13** 176 (1999)
40. Torii S et al. *Adv. Space Res.* **37** 2095 (2006), see p. 2098
41. Torii S et al. *Astrophys. J.* **559** 973 (2001)
42. Picozza P et al. *Astropart. Phys.* **27** 296 (2007)
43. Mocchiutti E, in *Proc. of the 30th Intern. Cosmic Ray Conf., Merida, México,* OG1.5 (2007) p. 1
44. Bocciolini M et al. *Nucl. Instrum. Meth. Phys. Res. A* **333** 560 (1993)
45. Boezio M et al. *Nucl. Instrum. Meth. Phys. Res. A* **487** 407 (2002)
46. Bocciolini M et al. *Nucl. Instrum. Meth. Phys. Res. A* **370** 403 (1996)
47. Boezio M et al. *Astropart. Phys.* **26** 111 (2006)
48. Bellotti R, Boezio M, Volpe F *Astropart. Phys.* **22** 431 (2005)
49. Casolino M et al. *Adv. Space Res.* **42** 455 (2008)
50. Ahn H S et al. *Adv. Space Res.* **37** 1950 (2006)
51. Chang J et al. *Adv. Space Res.* **42** 431 (2008)
52. Schmidt W K H et al., in *Proc. of the 26th Intern. Cosmic Ray Conf., Salt Lake City, UT, USA* Vol. 5 (Eds D Kieda, M Salamon, B Dingys) (1999) p. 41
53. Kossakowski R et al. "Electromagnetic calorimeter for the AMS-02 experiment", presented at *CALOR 2002, Pasadena, CA, March 25 – 29, 2002*
54. Ambrosi G *Nucl. Phys. B Proc. Suppl.* **125** 236 (2003)
55. Cadoux F et al. *Nucl. Phys. B Proc. Suppl.* **113** 159 (2002)
56. Plyaskin V V *Yad. Fiz.* **68** 61 (2005) [*Phys. At. Nucl.* **68** 60 (2005)]
57. Adloff C, in *Proc. of the 11th Intern. Conf. on Calorimetry in High-Energy Physics, Perugia, Italy, 2004*, p. 526
58. Hareyama M et al., in *Proc. of the 29th Intern. Cosmic Ray Conf., Pune* Vol. 3 (2005) p. 17
59. Asakimori K et al. *Astrophys. J.* **502** 278 (1998)
60. Torii S et al. *Nucl. Phys. B Proc. Suppl.* **134** 23 (2004)